ELSEVIER

Biophysical Chemistry 134 (2008) 10–19

Biophysical Chemistry

http://www.elsevier.com/locate/biophyschem

NMR comparison of the native energy landscapes of DLC8 dimer and monomer

P.M. Krishna Mohan [a], Maneesha Barve [a], Amarnath Chatterjee [a], Anindya Ghosh-Roy [b], Ramakrishna V. Hosur [a,*]

[a] *Department of Chemical Sciences, Tata Institute of Fundamental Research, Homi Bhabha Road, Mumbai 400 005, India*
[b] *Department of Biological Sciences, Tata Institute of Fundamental Research, Homi Bhabha Road, Mumbai 400 005, India*

Received 30 November 2007; received in revised form 24 December 2007; accepted 24 December 2007
Available online 12 January 2008

Abstract

Characterization of the low energy excited states on the energy landscape of a protein is one of the exciting and challenging problems in structural biology today. In this context, we present here residue level NMR description of the low energy excited states representing locally different alternative conformations in the dynein light chain protein, in its dimeric as well as monomeric forms. Important differences have been observed between the two cases and these are not necessarily restricted to the dimer interface. Simulations indicate that the low energy excited states are within a free energy of 2–3 kcal/mol above the native state. In both the monomer and the dimer the energy landscape is very sensitive to small pH perturbations. Nearly 25% of the residues (total of residues at pH 3.0 and 3.5 for the monomer, and at pH 7.0 and 6.0 for the dimer) access alternative conformations. The observations have been rationalized on the basis of protonation–deprotonation equilibria in the side chains; histidines in the case of the dimer and aspartates/glutamates in the case of the monomer. The possible relationship of the observed ruggedness of the native energy landscape with the protein structure, and its implications to protein adaptability and unfolding have been discussed.

Keywords: Dynein light chain protein; Low energy excited states; Energy landscape; Nuclear magnetic resonance; Unfolding initiation sites; Conformational fluctuations

1. Introduction

The stability and folding of a protein are intimately connected with the shape of its energy landscape. A deep well, the bottom of which corresponds to the native state would imply high stability of the native state. In contrast, a potential well with low lying excited states for the native state would have significant influence on the dynamics and functions of the protein. They also signify the structural adaptability, or susceptibility to unfolding in the presence of small external perturbations [1–13]. Thus, identification and characterization of such low energy excited states is a challenging and exciting problem in structural biology today.

NMR[$] chemical shift is a sensitive indicator of the environment and molecular conformation. In proteins ^{1}H, ^{13}C and ^{15}N chemical shifts are sensitive to protein secondary structures and are used to deduce the preliminary structural information [14–19]. The temperature dependence of amide proton chemical shifts in globular proteins has been investigated for over more than three decades by many researchers and continues to be investigated even today [20–27]. The amide proton chemical shifts are directly proportional to bond magnetic anisotropy (σ^{ani}) and this is crucially dependent on H-bonding, either intramolecular or inter-molecular. In the former case, the carbonyl groups, the H-bond acceptors play a crucial role. The bond magnetic anisotropy is proportional to r^{-3} where r is the

Abbreviations: NMR, nuclear magnetic resonance; HSQC, heteronuclear single quantum coherence; NOESY, nuclear overhauser enhancement spectroscopy; BMRB, Bio Mag Res Bank; IPTG, isopropyl-β-D-thiogalactopyranoside; PMSF, phenylmethulsulphonylfluoride; DLC8, dynein light chain protein; DTT, dithiothreitol; SDS-PAGE, sodium dodecyl sulphate Poly acrylamide gel electrophoresis; aa, amino acids.

* Corresponding author. Tel.: +91 22 2278 2488; fax: +91 22 2280 4610.
E-mail address: hosur@tifr.res.in (R.V. Hosur).

0301-4622/$ - see front matter © 2008 Elsevier B.V. All rights reserved.
doi:10.1016/j.bpc.2007.12.010

distance between the affected amide proton and the centre of the bond magnetic anisotropy, which lies close to the oxygen atom in the carbonyl groups [26]. In case of solvent accessible groups, H-bonding with solvent molecules influences the amide proton chemical shifts. Thus the amide proton chemical shift is critically dependent on the length of the H-bond the proton is engaged in.

When the temperature of the solution is raised, thermal fluctuations increase which results in an increase in the average distance between atoms; X-ray crystallographic studies at several temperatures (98–320 K) on ribonuclease-A indicated that the protein volume increases linearly with temperature to an extent of about 0.4% per 100 K [28]. Such an increase in the distance between the atoms participating in a H-bond results in weakening of the H-bond. Consequently, chemical shifts of most amide protons move upfield when the temperature is increased. Since bond magnetic anisotropy (σ^{ani}) is proportional to r^{-3} and molecular volume (V) is proportional to r^3, there is an inverse relationship of their variation with temperature ((σ^{ani})$\alpha 1/V$). However, over a small temperature range, (σ^{ani}) may appear to decrease linearly with temperature, and consequently amide proton chemical shifts would appear to vary linearly with temperature. In BPTI (basic pancreatic trypsin inhibitor) and lysozyme which are known to be extremely stable under a variety of extreme conditions, including temperature, it was indeed observed that the amide proton chemical shifts change linearly with temperature over the ranges, 279–359 K for BPTI and 278–328 K for lysozyme [21]. Such measurements have been carried out on many other proteins [27,29] and the temperature coefficients or the gradients of temperature dependence of the amide protons have been found to span a wide range, −16 to +4 ppb/K. For a strongly H-bonded amide this value is more positive than −4.5 ppb/K [21]. This is because the lengthening of the average H-bond distance will be greater for the inter-molecular H-bond, such as those with bulk water, than for the intra-molecular H-bonds.

However, if the protein structure is not very rigid, as would be the case for many systems, the chemical shifts would also be influenced by local structural and dynamics changes, and then the temperature dependence of chemical shifts may deviate from linearity. Indeed, in certain situations the amide proton chemical shifts have been seen to be non-linearly dependent on temperature, and this has been interpreted to indicate existence of alternative conformations the residues can access [30]. Identification of such residues provides a description of the energy landscape of the protein in the native state.

Cytoplasmic dynein, the principal minus end directed ATPase molecular motor has prominent role in various motility events [31–36]. Cytoplasmic dynein is a 1.2 MDa multi-subunit protein complex composed of various proteins ranging 10 kDa–600 kDa [34–37]. Among all the subunits dynein light chain protein (DLC8), a 10.3 kDa protein (89 residues) is the smallest subunit of the dynein motor complex. As DLC8 is present in all the functional dyneins, it is presumed to have an essential role in the regulation and assembly of the motor complex [38]. *Drosophila* DLC8 has 94%, 71%, and 50% sequence homology with DLC8 from human and rat, *Aspergillus nidulans* and yeast respectively. This high sequence similarity and evolutionary conservation indicates that the protein has multi-regulatory functions [39–41].

DLC8 is a dimer at physiological pH and a stable monomer below pH 4.0 [42,43]. The structures of both dimer and monomer have been solved [44,45]. The dimer is symmetrical and each monomer of the dimer consists of two α-helices (α1, residues 15–31; α2, residues 35–50) and five β-strands (β1, residues 6–11; β2, residues 54–59; β3, residues 62–67; β4, residues 72–78 and β5, residues 81–87) [44]. On the other hand the monomer consists of two α-helices (α1, residues 15–29; α2, residues 35–48) and four β-strands (β1, residues 8–11; β2, residues 55–58; β4, residues 72–78 and β5, residues 81–87) [45]. Thus the differences between the two structures are, (i) the β3 strand in the dimer loses its secondary structure on dissociation to the monomer, and (ii) the helices α1 and α2 and the strands β1 and β2 get shortened by two residues. The dimer binds the target molecules in an anti-parallel β-strand fashion through its β3-strand, whereas the monomer form of DLC8 is not capable of binding to target proteins [43]. This property is expected to have a regulatory role in the protein function.

We have characterized here the low energy excited states of both the dimeric and the monomeric forms of DLC8 in their native state ensembles. This was based on the temperature dependence of the amide proton chemical shifts. We also investigated the effects of small pH perturbations on the extent and nature of the temperature dependences. The residues accessing alternative conformations in the dimer and the monomer are seen to be somewhat different in some segments, although there are many commonalities as well. These sites could be the most susceptible sites for local unfolding in the protein structure, and would also represent the sites of structure adjustment when required by the environmental perturbations.

2. Materials and methods

2.1. Overexpression and protein purification

The plasmids (vector pETI4B) harboring the gene for the His tagged DLC8 were transformed into *Escherichia coli* BL21(DE3) host cells for protein expression. The M9 minimal medium (with and without ^{13}C labeled glucose) containing $^{15}NH_4Cl$ and ampicillin (100 μg/ml) was inoculated with recombinant BL21(DE3) cells. From an overnight seed culture, a big culture (1 l) was grown at 37 °C to an OD_{600} of 0.6 to 0.8. Expression of protein was induced with a final concentration of 600 μM of IPTG, and the culture was incubated at 37 °C for another 6 h. The cells were harvested by centrifugation at 5500 RPM for 30 min. The harvested culture was lysed using extraction buffer (20 mM Tris, 10 mM imidazole, 200 mM NaCl, pH 8) containing 50 μl leupeptin (1.25 mg/ml H_2O), 50 μl pepstatin (0.5 mg/ml DMSO or methanol), 50 μl PMSF (50 mM iso-propanol), 1% Triton X, 50 μl lysozyme (50 mg/ml H_2O). The lysed cells were sonicated and spun at 35,000 rpm for 45 min to obtain a clear supernatant. The protein was then purified using a Ni-

chelating column. His tag was cleaved by incubating the protein on the beads with thrombin for 12 h at room temperature. DLC8 monomer was obtained by exchanging the protein with pH 3 buffer (20 mM acetate, 200 mM NaCl, 2 mM DTT). The purity of the sample was checked using SDS-PAGE. A protein sample in which the arginines were selectively unlabelled was prepared following previously reported procedure [46].

2.2. Gel filtration

Gel filtration was performed at pH 7.0, 6.0, 3.5 and 3.0 using a Hi Load 16/60 Superdex 75 column (Amersham) with buffer (20 mM phosphate, 200 mM NaCl, 2 mM DTT at pH 7.0, 6.0; 20 mM acetate, 200 mM NaCl, 2 mM DTT at pH 3.5 and 3.0) at a flow rate of 1.0 ml/min with absorbance monitored at 280 nm using Bio-Rad BioLogic LP system. Nearly 1 ml of 600 μM protein was loaded on to the column.

2.3. Circular dichroism

Thermal stability of DLC8 dimer and monomer was measured by recording far-UV CD spectra at 222 nm as a function of temperature in the range 293 K to 318 K on a JASCO model J-810 spectropolarimeter using a bandwidth of 1 nm. Protein concentration of 40 μM in phosphate buffer (20 mM phosphate, 200 mM NaCl, 2 mM DTT at pH 7.0) and acetate buffer (20 mM acetate, 200 mM NaCl, 2 mM DTT at pH 3.0) was used in a fused quartz cell with a path length of 0.1 cm for dimer and monomer experiments respectively. Data was collected in a continuous mode at a rate of 1 K per minute. Data was smoothened by three point averaging to minimize errors due to thermal fluctuations.

2.4. NMR spectroscopy

2.4.1. NMR sample

For NMR studies the protein purified as described above was concentrated to 1.0 mM. Phosphate buffer (20 mM phosphate, 200 mM NaCl, 2 mM DTT) and acetate buffer (20 mM acetate, 200 mM NaCl, 2 mM DTT), were used for the 2D experiments on the dimer (pH values 7.0, 6.0) and on the monomer (pH values 3.5 and 3.0) respectively. The final volume in all the samples was ~550 μl (90% H_2O+10% D_2O).

2.4.2. NMR data acquisition and processing

All the NMR experiments were recorded using a triple channel Varian Unity-plus 600 MHz NMR spectrometer equipped with pulse-shaping and pulse field gradient capabilities. For resonance assignments a series of 3D experiments HNCA, HN(CO)CA, CBCANH and CBCA(CO)NH [47,48] were recorded at pH 7.0, 27 °C. NOESY-HSQC was recorded at all the four pH values (pH 7.0, 6.0, 3.5 and 3.0) with a mixing time of 150 ms, 40 complex points along ^{15}N (t_1) dimension and 64 complex points along ^{1}H (t_2) dimension. For the triple resonance experiments the ^{1}H and ^{15}N carrier frequencies were set at 4.71 ppm and 119 ppm respectively. The ^{13}C carrier frequency was set at 56.0 ppm for HNCA and HN(CO)CA, and at 46.0 ppm for CBCANH and CBCA(CO)NH. Amide proton chemical shifts as a function of temperature in the range 290–315 K were measured by recording seven HSQC spectra (293 K, 296 K, 300 K, 303 K, 306 K, 309 K, 312 K) with 160 t_1 increments each. Both the dimer and the monomer were stable over the entire temperature range at all the pH values. ^{1}H chemical shifts were calibrated relative to 2,2-dimethyl-2-silapentane-5-sulfonate (DSS).

All the data were processed using FELIX on a Silicon Graphic, Inc. work station. Prior to Fourier transformation and zero filling, data was apodized with a sine-squared weighting function shifted by 60° in both dimensions for 2D and by 90° in all dimensions for 3D experiments. After zero filling and Fourier transformation the final matrix had 1024, 256 and 256 points along the F_3, F_2 and F_1 dimensions, respectively, and the 2D HSQC experiments had 4096, 1024 points, respectively, along the F_2 and F_1 dimensions. The digital resolution in the spectra was ~1.7 Hz/point along F_2. The chemical shift assignment was done using the peak picking macro of Felix which finds the peak maximum using an interpolation procedure. Chemical shifts were first calculated and fitted to a straight line after which the deviations from linearity were used to derive the residual curvatures. As a measure of curvature, the experimental data (or, equivalently, the residuals from the linear fitting) were fitted to a parabola, by using Marquardt non-linear least-squares fitting. All protons for which the second-order coefficient (c in the equation $y=a+bx+cx^2$) differed from zero (using a ^{1}H chemical shift error of ±0.004 ppm) were treated as having curved temperature dependence [8].

2.5. Simulations

Simulations of the temperature dependence of changes in backbone $^{1}H^{N}$ chemical shifts were carried out as described by Williamson et al. [30] using Sigma Plot 8.0 in the temperature range 290 K–315 K. We assumed a ground state shift of 8.5 ppm, with a typical hydrogen-bonded temperature gradient of −2 ppb/K, [21] and an alternative state shift of 8.0 ppm, with a typical non-hydrogen-bonded gradient of −7 ppb/K. Mulder et al. [49] who measured an excited state in the L99A mutant of T4 lysozyme, characterized by ΔG=2 kcal/mol, ΔH=7.1 kcal/mol, and $T\Delta S$ (298 K)=5.1 kcal/mol. Hence we used these values as illustrative estimates. Thus, the values used for the different thermodynamic parameters during calculations are, $T\Delta S$ (298 K)=5.1 kcal/mol which is equivalent to ΔS= 17.2 cal/mol K^{-1}, and ΔH=6.1 kcal/mol, ΔH=7.1 kcal/mol, ΔH=8.1 kcal/mol, ΔH=9.1 kcal/mol corresponding to difference in the free energy (ΔG) at 298 K of 1, 2, 3 and 4 kcal/mol, respectively. The shifts (δ) and gradients (g) for the native state (δ_1, g_1) and excited state (δ_2, g_2) used for the above calculations are δ_1=8.5 ppm, δ_2=8.0 ppm, and g_1=−2 ppb/K, g_2=−7 ppb/K for convex shapes and δ_1=8.0 ppm, δ_2=8.5 ppm, and g_1=−7 ppb/K, g_2=−2 ppb/K for concave shapes. In all the simulations, chemical shifts have been first calculated and fitted to a straight line. Then, the deviations from the linearity have been used to derive the residual curvatures.

3. Results

3.1. Resonance assignments

Backbone assignment in the DLC8 dimer at pH 7, 27 °C was achieved by a combination of several conventional three dimensional triple resonance experiments [47,48,50]. Assignment of arginines at positions 4 and 71 was facilitated by a $^{1}H–^{15}N$ HSQC recorded on a protein which was uniformly ^{15}N label1ed but for the arginines. Assignments at pH 6 were obtained by direct transfer from assignments at pH 7. Sequence specific assignments at pH 3 were obtained using the standard experiments [50] in conjunction with HNN and HN(C)N experiments [51]. Then, HSQC peak assignments at pH 3.5 were derived from simple transfer from those at pH 3. However, on few occasions where small movements of peaks resulted in some ambiguities, the assignments were confirmed from observation of sequential NOE connectivities in the $^{1}H–^{15}N$ NOESY-HSQC spectra.

3.2. Thermal stability of DLC8 protein

We carried out thermal stability studies on the DLC8 dimer (pH 7) and monomer (pH 3) [52] to assess the temperature range where one can reliably study the temperature dependence of the amide proton chemical shifts without significantly perturbing the structures. The thermal stability data for both the dimer and the monomer are shown in Fig. 1. It is evident that both the dimeric and monomeric structures are very stable over the temperature range, 293–318 K used in the present study.

3.3. Temperature dependence of amide proton chemical shifts

We observed that amide proton chemical shifts for several residues in DLC8 exhibited non-linear dependence on temperature, and as described in the Introduction this must be interpreted to indicate the existence of alternate conformations (low energy excited states), the residues can access [8,53]. In order to understand the parameters that influence such conformational fluctuations, we theoretically simulated the temperature dependence of amide proton chemical shifts and compared them with the experimental results obtained in the temperature range 290–315 K.

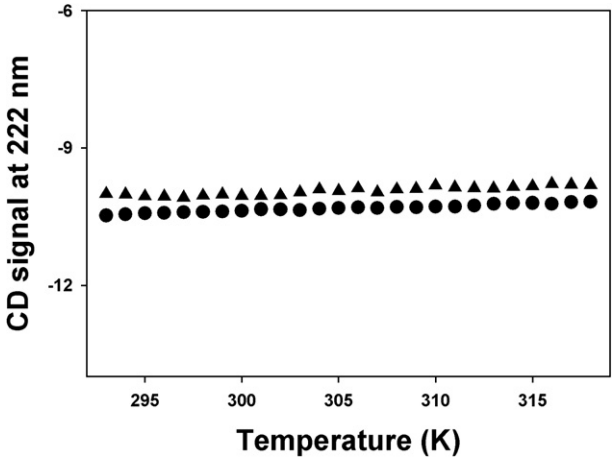

Fig. 1. Thermal stability of DLC8 dimer (pH 7, circles) and monomer (pH 3, triangles) monitored by far-UV CD at 222 nm in the temperature range 293–318 K.

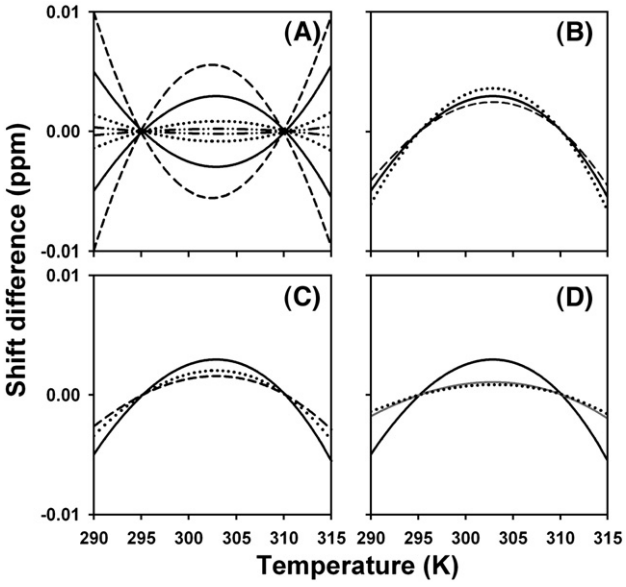

Fig. 2. Simulations of the dependence of H^N chemical shift variation with temperature (290 K–315 K). In all the calculations shown chemical shifts are calculated and fitted to a straight line. Then the deviations from linearity are used to derive the residual curvatures. (A) Different curves show the dependence on free-energy difference between the native and the higher energy alternate state: ΔG=1 kcal/mol (dashed), ΔG=2 kcal/mol (solid), ΔG=3 kcal/mol (dotted) and ΔG=4 kcal/mol (dash double dot dash); for these $T\Delta S$ at 298 K was fixed at 5.1 kcal/mol and ΔH varied as 6.1, 7.1, 8.1, and 9.1 kcal/mol respectively. The chemical shift and gradient parameters are: δ_1=8.5 ppm, δ_2=8.0 ppm, and g_1=−2 ppb/K, g_2=−7 ppb/K for convex shapes and δ_1=8.0 ppm, δ_2=8.5 ppm, and g_1=−7 ppb/K, g_2=−2 ppb/K for concave shapes. (B) The solid curve is the same as in 'A' (ΔG=2 kcal/mol); dashed curve, δ_1=8.1 ppm, δ_2=8.0 ppm, g_1=−2 ppb/K, g_2=−7 ppb/K, ΔG=2 kcal/mol; dotted curve, δ_1=9.0 ppm, δ_2=8.0 ppm, g_1=−2 ppb/K, g_2=−7 ppb/K, ΔG=2 kcal/mol. (C) The solid curve is the same as in 'A' (ΔG=2 kcal/mol); dashed curve, δ_1=8.5 ppm, δ_2=8.0 ppm, g_1=−2 ppb/K, g_2=−4 ppb/K, ΔG=2 kcal/mol; dotted curve, δ_1=8.5 ppm, δ_2=8.0 ppm, g_1=−4 ppb/K, g_2=−7 ppb/K, ΔG=2 kcal/mol. (D) The solid black curve (ΔG=2 kcal/mol) and the dotted curve (ΔG=3 kcal/mol) are the same as in 'A'; solid grey curve is for δ_1=8.1 ppm, δ_2=8.0 ppm, g_1=−2 ppb/K, g_2=−4 ppb/K with ΔG=2 kcal/mol.

3.3.1. Theoretical simulations

Consider a residue having two conformational states accessible to it i.e., a native state and a higher energy state. Following the discussion in the Introduction, each of them can be assumed to have a linear variation of chemical shift with temperature as, $\delta_1 = \delta^o{}_1 + g_1 T$ and $\delta_2 = \delta^o{}_2 + g_2 T$, where g_1 and g_2 are the gradients of temperature dependence, δ_1 and δ_2 are the chemical shifts of the native and the excited states respectively, and T is the temperature. If P_1 and P_2 are the corresponding populations of the native and the excited states, the observed chemical shift, δ_{obs}, of the amide proton will be given by,

$$\delta_{obs} = \delta_1 P_1 + \delta_2 P_2.$$

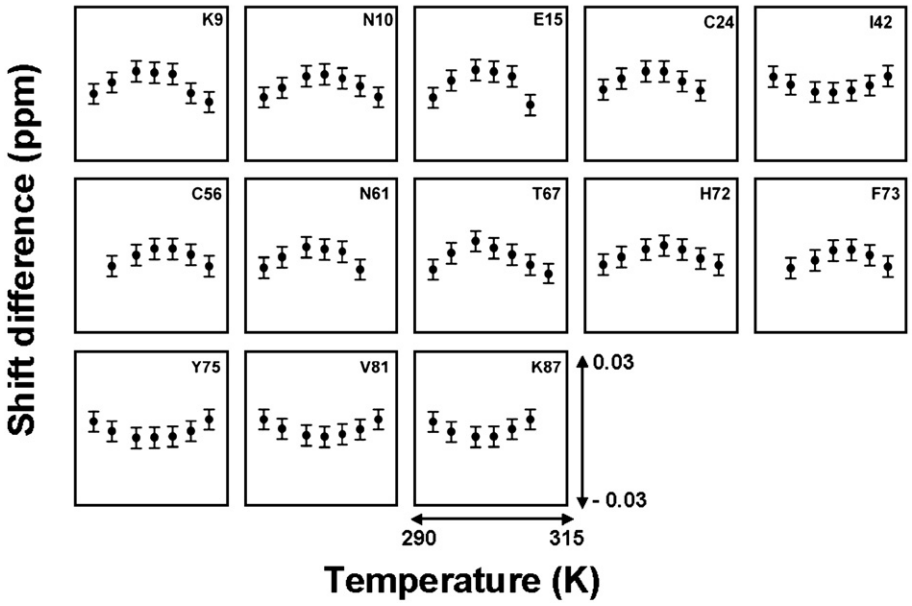

Fig. 3. Residues showing non-linear temperature dependence of amide proton chemical shifts in DLC8 measured at pH 7.0. The measured chemical shifts were fitted to a linear equation. The residuals (observed value — calculated value according to the linear fit) have been plotted against temperature; total scale of y-axis is 0.06 ppm: +0.03 to −0.03 centered at zero, and the temperature range is 290 K–315 K. The error bars give an indication of the approximate error in measured chemical shifts (±0.004 ppm).

These populations depend on the free-energy difference between the two states. If there are more states contributing, then the observed shift will be a weighted average over all the accessible states. It is this complex dependence of chemical shifts on many thermodynamic and other factors, which leads to non-linear dependence of chemical shifts on temperature. To understand the influence of these factors we performed simulations of H^N chemical shift variation with temperature in the range, 290 K–315 K, using a two state model [30] following the parameters described in Materials and methods.

$$\delta_{\mathrm{obs}} = \frac{\left(\delta_1^0 + g_1 T\right) + \left[\left(\delta_2^0 + g_2 T\right) e^{-(\Delta G/\mathrm{RT})}\right]}{1 + e^{-(\Delta G/\mathrm{RT})}}$$

where, ΔG is the free-energy difference between the two states, and $\Delta G = \Delta H - T\Delta S$, where, ΔH and ΔS are the enthalpy difference and the entropy difference respectively. The results of the simulations are shown in Fig. 2. Fig. 2A shows the curves for ΔG ranging from 1–4 kcal/mol keeping the gradients and chemical shifts of the native and the excited states constant. Here, it is worthwhile to note that in the chosen temperature range (290 K–315 K) the curvature almost disappears above $\Delta G = 3$ kcal/mol. Fig. 2B and C show the dependence of curvature on chemical shift differences and gradient differences respectively, between the native and the excited states, when ΔG is held constant ($\Delta G = 2$ kcal/mol). In Fig. 2B, three values of δ_1: 8.5 (reference), 8.1 and 9.0 are considered, keeping the other parameters the same as in Fig. 2A for convex shape of curvature. Similarly, in Fig. 2C, three combinations of gradients: (g_1, g_2) (ppb/K)=(−2, −7) (reference), (−2, −4) and (−4, −7) are considered keeping the other parameters same as in Fig. 2A for convex shape of curvature. From these it is evident that neither the chemical shift difference nor the difference in gradients, by itself changes the curvature to a noticeable extent. Next, we carried out a simulation for a combination of changes in 'chemical shift difference' and 'gradient difference' (δ_1 = 8.1 ppm, δ_2 = 8.0 ppm, g_1 = −2 ppb/K, g_2 = −4 ppb/K) keeping the free-energy constant ($\Delta G = 2$ kcal/mol). This is shown by solid grey line in Fig. 2D. Interestingly, this curve almost exactly overlaps with the curve for which $\Delta G = 3$ kcal/mol in Fig. 2A which has a lower curvature compared to that of the curve with $\Delta G = 2$ kcal/mol; for ease of comparison, the corresponding curve from Fig. 2A is redrawn in Fig. 2D as a dotted line. This clearly suggests that although the appearance of curvature confirms the presence of alternative states, the lack of curvature does not necessarily imply the absence of low energy excited states. These results will be of great help for interpreting the experimental results on temperature dependence of amide proton chemical shifts.

3.3.2. Low energy excited states in the dimer and the monomer

We measured temperature dependence of the amide proton chemical shifts in the DLC8 dimer (pH 7) and in the monomer (pH 3) by recording HSQC spectra as a function of temperature in the range 290–315 K. The experiments were restricted to 315 K in order to be in the temperature range which is far below the point of aggregation in the case of the dimer and also to be well below the onset of unfolding for the monomer. Here, it is worthwhile to mention that the HSQC spectra measured at all the temperatures for both the monomer and the dimer are qualitatively similar suggesting that indeed no structural changes occur in the native state in the whole range. The individual temperature dependences of the amide proton chemical shifts were analyzed by fitting the chemical shifts to a

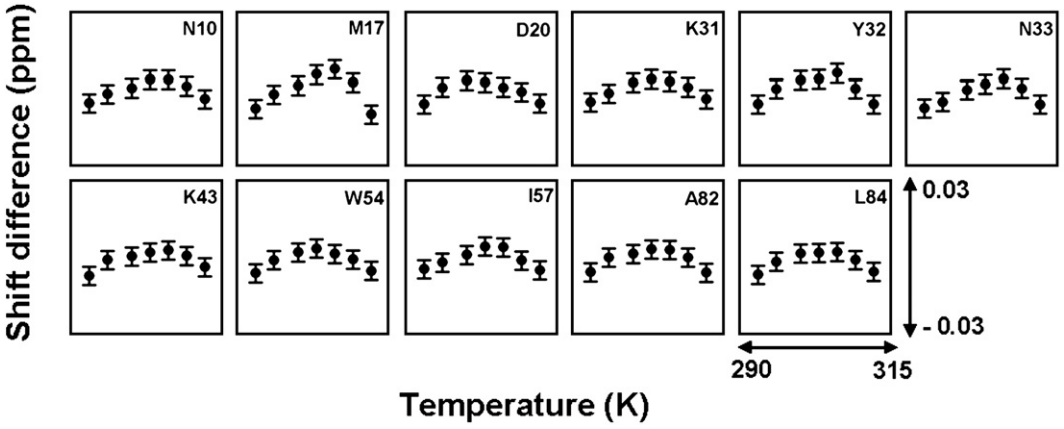

Fig. 4. Residues showing non-linear temperature dependence of amide proton chemical shifts in DLC8 measured at pH 3.0. The measured chemical shifts were fitted to a linear equation. The residuals (observed value — calculated value according to the linear fit) have been plotted against temperature; total scale of *y*-axis is 0.06 ppm: +0.03 to −0.03 centered at zero, and the temperature range is 290 K–315 K. The error bars give an indication of the approximate error in measured chemical shifts (±0.004 ppm).

straight line. Then the deviations from linearity were used to derive the residual curvatures, and the uncertainties were calculated as described in Materials and methods. In our data several residues exhibited curved dependence while others displayed linear behavior with temperature. All the residues in the dimer at pH 7 that deviated from linearity are shown in Fig. 3. The curvatures are different for different residues and we observe both convex and concave shapes. As described in the simulations, the major determinant of the shape of curvature is the relative magnitude of the amide proton chemical shift of the native state vs that of the alternative state the particular residue accesses [30]. Thus, the convex and concave shapes reflect on different kinds of structural perturbations in the low energy excited states.

Similarly, Fig. 4 shows the residues that are accessing low energy excited states in the DLC8 monomer at pH 3. Comparison of Figs. 3 and 4 reveals that the residues accessing alternative conformations, and so also the natures of the excited sates (as depicted by concave or convex shapes, magnitudes of curvature etc.,) have many differences between the dimer and the monomer. In the background of the simulations described above, the magnitudes and the patterns of the experimentally observed curvatures indicate that the alternative conformations accessed by each residue lie within ~2.5 kcal/mol from the native state.

3.3.3. pH sensitivity

Application of small environmental perturbations such as small concentrations of chemical denaturants, change in pressure, pH change etc., is often useful to investigate the preferential sensitivities of different residues to external perturbations, while the protein itself remains entirely in the native state ensemble [30,54]. In fact, these environment sensitive residues are those which play prominent roles in various biological activities such as signal transduction, enzymatic catalysis, macromolecular association, cargo trafficking, etc. Among the above mentioned environment perturbations, pH variation is a mild perturbation and in general it changes the protonation states of the various residues depending on the chosen pH range. In order to identify the pH sensitive conformational dynamics in DLC8 protein we measured the temperature dependence of the amide proton chemical shifts in both the dimer and the monomer at slightly different pH conditions i.e., dimer at pH 6 and monomer at pH 3.5.

It is known that DLC8 exhibits a pH induced dimer-to-monomer transition in between pH 7 and pH 3 with a transition midpoint of pH 4.5 [42,55]. Therefore it is important to confirm that the protein remains a pure dimer at pH 6 and a pure monomer at pH 3.5. To examine this aspect we performed gel filtration experiments at a low concentration (~100 μM), and also at a higher concentration (~600 μM) of the protein. The latter is almost at the NMR concentration. The results at both the concentrations were identical and Fig. S1 of Supplementary material shows a superposition of the chromatograms recorded at pH 3 and 3.5 and at the higher value of the protein concentration mentioned. Clearly, the protein elutes as a single peak

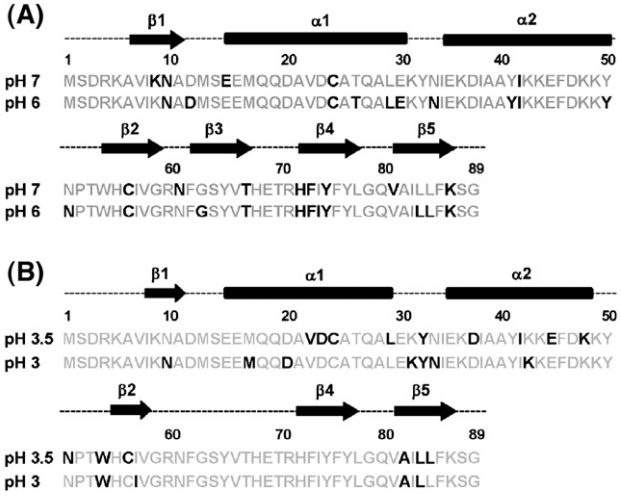

Fig. 5. Residues showing non-linear temperature dependence of amide proton chemical shifts (black) along the polypeptide chain. The results are shown for pH 7.0 and 6.0 (A) and for pH 3.5 and 3.0 (B). The arrows (β strands) and cylinders (α helix) indicate native secondary structures.

with equal width suggesting the existence of single species (pure monomer). We made similar observations at pH 7 and 6, which we published recently in a different context [56] and thus do not wish to repeat that data here. Thus, we conclude that the differences observed in the sites of conformational fluctuations at pH 6 and 3.5 from those at pH 7 and 3 respectively, are due to the local environmental perturbations. All the residues accessing such low energy excited states in the dimer at pH 6 are shown in Fig. S2 (see Supplementary material) and those in the monomer at pH 3.5 are shown in Fig. S3 (see Supplementary material). A summary of all these results at various pH values i.e., pH 7 and 6 for the dimer and pH 3.5 and 3 for the monomer is shown in Fig. 5. The number of residues accessing alternative conformations in the dimer at pH 7 and 6 are 13 and 21 respectively (Fig. 5A). Fig. 6A and B displays the locations of these residues on the native structures [57] of the protein. Likewise, the number of residues accessing alternative conformations in the monomer at pH 3.5 is 15 and that at pH 3 is 11 (Fig. 5B). The locations of these residues are marked with red color on the native structure of the monomeric protein in Fig. 6C and D respectively [45]. The differences in the low energy excited states detected at pH 6 as compared to those at pH 7, and at pH 3.5 as compared to those at pH 3 must be attributed to the changes in the protonation states of the various side chains in the measured pH range (see below).

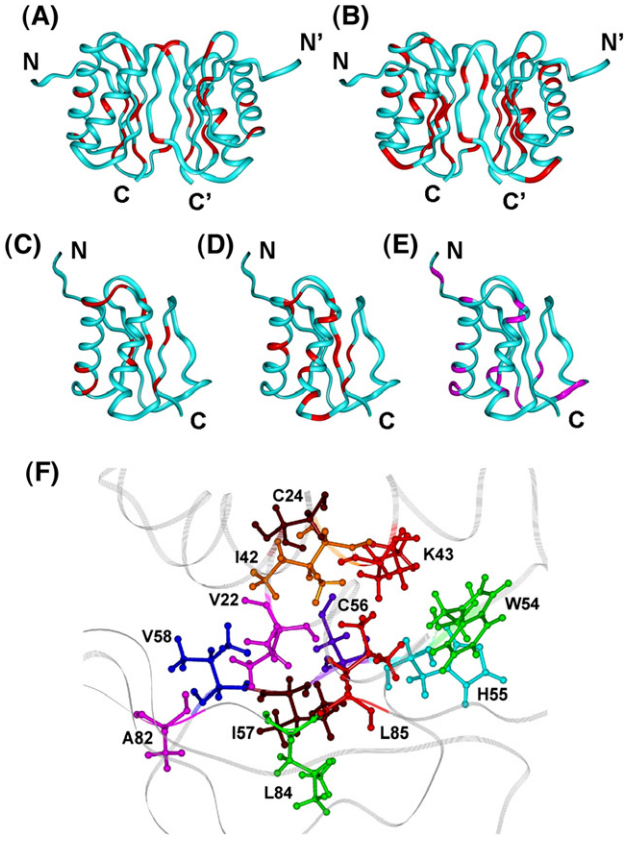

Fig. 6. Residues exhibiting curved temperature dependence in DLC8 dimer (A) pH 7.0, (B) pH 6.0 (PDB Id: 1f3c) and in monomer (C) pH 3.0, (D) pH 3.5 (PDB Id: 1rhw), are colored red on the three dimensional structure of the protein. (E) Positions of all the titratable groups in the pH range 7.0 to 3.0 (aspartates, glutamates and histidines) are marked with pink color on the monomer structure (PDB Id: 1rhw). (F) Zooming in on a particular region surrounding β2 strand in the NMR structure of the monomer (PDB Id: 1rhw) to show the side-chain interactions. Only a few residues in α1, α2 and β5 are shown for the sake of clarity. DLC8 monomer image was produced using Insight II.

Table 1
Comparison of number of residues accessing alternative conformation in structural regions in DLC8 dimer and monomer

Structural element	Number of residues accessing alternative conformations	
	Dimer	Monomer
α1	5	6
α2	3	5
β1	2	1
β2	1	3
β3	2	–
β4	4	0
β5	3	3

4. Discussion

4.1. Native state energy landscape of DLC8

As mentioned earlier identification of the residues accessing alternative conformations provides a description of the native state energy landscape of the protein. While the pH sensitivity of conformational dynamics indicates, on one hand, finer adjustments at residue level, the results at both the pH values (7 and 6 for the dimer and 3 and 3.5 for the monomer) put together indicate the overall vulnerabilities in the native state, since neither of the pH perturbations take the protein out of the native state ensemble. Overall, the numbers for residues which can access alternative conformations considering either of the pH values are: 25 for dimer and 22 for monomer (Fig. 5), which is around 25% of the total number of residues in the protein. Table 1 provides a comparison to indicate the differences in the number of residues accessing alternative conformations in the various structural elements in the dimer and the monomer. It is interesting to see that the residues that access alternative conformations in the dimer and the monomer are somewhat different in different regions (Fig. 5), although the dimer and the monomer have nearly same secondary and tertiary folds [45]. Importantly, the differences are not necessarily restricted to the dimer interface. The N-terminal helices are more dynamic in the monomer whereas the C-terminal β-sheets are more dynamic in the dimer. Similarly, many residues which are dynamic in the α1 and α2 helices in the monomer lose this dynamic nature in the dimer (Table 1), and likewise, several residues which are not dynamic in the β4 strand in the monomer acquire dynamic character in the dimer (Fig. 5). It is also important to mention here that the lack of curvature or the presence of linearity does not necessarily indicate the lack of alternative states; the linear or non-linear behavior is a complex interplay of chemical shift gradients of the ground and the alternative states, magnitudes of the shift differences between the two states, and temperature dependence of the free-energy difference between the two states [30]. Even so, it is clear that a large number of residues in DLC8

access alternative conformations, both in the dimer and in the monomer.

The differences observed in the positions of the residues accessing alternative conformations in the dimer and in the monomer due to small pH perturbations provide insights into the sensitivity of the conformational fluctuations due to environment perturbations in the two cases. In fact, the perturbation of the dimer landscape would have functional significance since small pH differences are known to exist in different parts of a cell [58–62]. It is evident from Fig. 6A and B that several of the residues that access low energy excited states are surrounding the dimer interface of the molecule which is also the cargo binding site [44]. It can be envisaged that the observed sensitivity of conformational dynamics at the dimer interface due to small environmental perturbations can significantly influence the cargo binding nature of the protein. Likewise, in the monomer (Fig. 6C and D) [45], noticeable differences have been observed in both α1 and α2 helices. Interestingly, the α2 helix participates in several inter-monomer contacts once the dimer is formed and hence its sensitivity to small perturbations may have a crucial role for the proper formation of the functional dimer.

Another important point to be noted at this stage is that there are many differences in the energy landscapes of the dimer and the monomer of DLC8 (Table 1 and Fig. 6A–D). The differences are not just restricted to the dimer interface. This implies that the structural perturbations caused by dimer formation travel through the protein structure via side-chain interactions and this then causes local changes in the protein dynamics.

These results augment the conclusions previously derived from relaxation measurements [42] on DLC8 dynamics at different time scales. The present data provides information on the ranges of free energies of the near native states accessed by the fluctuating residues and indicate that for those which exhibit curvature in the temperature dependence of amide proton chemical shifts, the alternative states lie within 2–3 kcal/mol from the ground state.

4.2. Relationship between sequence, structure and pH sensitivity of DLC8 landscapes

The roughness of the energy landscape and the consequent fluctuations in the native state of a protein is a reflection on the nature of the interactions between the side chains of the different amino acid residues in the three dimensional structure of the protein. While this is not generally predictable, some insights may be obtained in some cases by closely examining the structure and the properties of the amino acids along the sequence. For example, the behaviors of residues with titratable groups, which are likely to be affected by a pH perturbation, can provide useful clues. An observed perturbation at such locations would indicate that conformational fluctuations could be arising due to existence of species with different protonation states; a change in the protonation state of a side chain causes a local change in the electrostatic potential, and thereby results in some population of an alternative conformation on energetic considerations. Inter-conversion between the major population and the minor population so created leads to the so-called conformational fluctuations.

In the above background it is interesting to note that most of the residues with titratable groups in the side chains in DLC8 (Fig. 6E) are located in the regions which are exhibiting conformational fluctuations, and hence, their perturbation by small pH changes provides useful mechanistic insights. In the case of the dimer, the sensitivity of conformational dynamics can be readily traced to partial protonation of the His side chains as described earlier [42]. There will be inter-conversions between charged and neutral His and there will also be charge–charge repulsions. These will cause fluctuations in local electrostatic potentials and consequently in local side chain packing, which in turn will affect the main chain conformations. Among the three histidines, His 55 (pK 4.5, [55]), His 68 and His 72 (both have pK of 6.0, [55]), the latter two would be the major contributors to the observed differences in the fluctuations of the native state in the pH range of 6–7.

In the case of DLC8 monomer His 68 and His 72 do not have any effect on the observed differences as they are completely protonated below pH 4.0. On the other hand His 55 (pK 4.5, [55]), would have a significant effect. At pH 3.5 the side chain of His 55 will be protonated to the extent of 90% and exchange between protonated and free His will contribute to a local dynamics. The environmental perturbation due to this dynamics would get relayed through the β2 strand and the α1, α2 helices and the β5 strand due to the close packing of the side chains in the protein structure (Fig. 6F). The side chains for a few residues of α1, α2 and β5 are shown in the figure and all of these residues are seen to exhibit curved temperature dependence. At pH 3.0, the population of protonated His will increase and this results in the observed perturbation differences. Similarly, the perturbations at the other titratable groups such as aspartates and glutamates in the α1 and α2 helices (see Fig. 6E) would also cause local relays and contribute to the accessibility of different low energy excited states. All these influence the native energy landscape of the protein.

4.3. Potential unfolding initiation sites in the DLC8 monomer

The roughness of the native energy landscape of a protein would also have repercussions on the unfolding pathways of the protein. Baxter et al. [53] suggested that the alternative states are the most probable candidates for the earliest cooperative unfolding events which might further develop into partially unfolded forms. On these grounds, the following sites: Val 22, Asp 23, Cys 24, Leu 29 in the α1 helix; Lys 31, Phe 32, Asp33, in the α1–α2 loop; Asp 37, Ile 42, Lys 43, Glu 45, Lys 48 in the α2 helix; Cys56, Ile 57 in the β2 strand and Ala 82, Leu 84, Leu 85 in the β5 strand may be identified as potential unfolding initiation sites for the protein. These results in conjunction with those derived from relaxation data [63] which monitor conformational exchange at ms–μs time scale suggest that unfolding in DLC8 can start from many different locations in the protein structure and these include both structured and flexible areas.

5. Conclusions

We have obtained here residue level view of the low energy excited states of both the dimeric and the monomeric forms of the dynein light chain protein. Significant differences are seen in the native energy landscapes of the dimer and the monomer although they have similar structural topologies. The differences are not necessarily restricted to the dimer interface. This has a bearing on the side-chain packing and the relay of perturbations through the protein structure. It is interesting to note that the conformational dynamics observed for several residues both in the dimeric and in the monomeric forms are environment sensitive. His 68 and His 72 side chains contribute in the observed differences in the dynamic character in the dimer, whereas His 55 and other residues with carboxylic acid side chains are the major contributors for the monomer. The roughness of the dimer energy landscape provides rationales for the adaptability of the protein structure to bind various cargo molecules in order to carry out the cargo trafficking in an efficient manner. On the other hand, the results obtained for the monomer throw light on the formation of a stable functional dimer as the α2 helix and the β2 strand participate in a number of inter-monomer contacts in the DLC8 dimer. The monomer results also provide insights into the many potential unfolding initiation sites in the protein.

Acknowledgement

We thank the Government of India for providing financial support to the National Facility for High Field NMR at the Tata Institute of Fundamental Research. PMKM is a recipient of the TIFR Alumni Association Scholarships (2003–2005) for career development and Sarojini Damodaran international fellowships supported by the TIFR endowment fund.

Appendix A. Supplementary data

Supplementary data associated with this article can be found, in the online version, at doi:10.1016/j.bpc.2007.12.010.

References

[1] P.K. Agarwal, Role of protein dynamics in reaction rate enhancement by enzymes, J. Am. Chem. Soc. 127 (2005) 15248–15256.
[2] V.A. Feher, J. Cavanagh, Millisecond-timescale motions contribute to the function of the bacterial response regulator protein Spo0F, Nature 400 (1999) 289–293.
[3] R. Nevo, V. Brumfeld, R. Kapon, P. Hinterdorfer, Z. Reich, Direct measurement of protein energy landscape roughness, EMBO Rep. 6 (2005) 482–486.
[4] F.G. Parak, Proteins in action: the physics of structural fluctuations and conformational changes, Curr. Opin. Struck. Biol. 13 (2003) 552–557.
[5] S. Piana, P. Carloni, M. Parrinello, Role of conformational fluctuations in the enzymatic reaction of HIV-1 protease, J. Mol. Biol. 319 (2002) 567–583.
[6] G.R. Stockwell, J.M. Thornton, Conformational diversity of ligands bound to proteins, J. Mol. Biol. 356 (2006) 928–944.
[7] D. Tobi, I. Bahar, Structural changes involved in protein binding correlate with intrinsic motions of proteins in the unbound state, Proc. Natl. Acad. Sci. U. S. A. 102 (2005) 18908–18913.
[8] R.B. Tunnicliffe, J.L. Waby, R.J. Williams, M.P. Williamson, An experimental investigation of conformational fluctuations in proteins G and L, Structure 13 (2005) 1677–1684 (Camb.).
[9] S.T. Whitten, E.B. Garcia-Moreno, V.J. Hilser, Local conformational fluctuations can modulate the coupling between proton binding and global structural transitions in proteins, Proc. Natl. Acad. Sci. U. S. A. 102 (2005) 4282–4287.
[10] Y.O. Kamatari, S. Yokoyama, H. Tachibana, K. Akasaka, Pressure-jump NMR study of dissociation and association of amyloid protofibrils, J. Mol. Biol. 349 (2005) 916–921.
[11] D.D. Boehr, D. McElheny, H.J. Dyson, P.E. Wright, The dynamic energy landscape of dihydrofolate reductase catalysis, Science 313 (2006) 1638–1642.
[12] E.Z. Eisenmesser, O. Millet, W. Labeikovsky, D.M. Korzhnev, M. Wolf-Watz, D.A. Bosco, J.J. Skalicky, L.E. Kay, D. Kern, Intrinsic dynamics of an enzyme underlies catalysis, Nature 438 (2005) 117–121.
[13] A. Mittermaier, L.E. Kay, New tools provide new insights in NMR studies of protein dynamics, Science 312 (2006) 224–228.
[14] S. Schwarzinger, G.J. Kroon, T.R. Foss, P.E. Wright, H.J. Dyson, Random coil chemical shifts in acidic 8 M urea: implementation of random coil shift data in NMRView, J. Biomol. NMR 18 (2000) 43–48.
[15] S. Schwarzinger, G.J. Kroon, T.R. Foss, J. Chung, P.E. Wright, H.J. Dyson, Sequence-dependent correction of random coil NMR chemical shifts, J. Am. Chem. Soc. 123 (2001) 2970–2978.
[16] D.S. Wishart, B.D. Sykes, F.M. Richards, Relationship between nuclear magnetic resonance chemical shift and protein secondary structure, J. Mol. Biol. 222 (1991) 311–333.
[17] D.S. Wishart, B.D. Sykes, F.M. Richards, The chemical shift index: a fast and simple method for the assignment of protein secondary structure through NMR spectroscopy, Biochemistry 31 (1992) 1647–1651.
[18] D.S. Wishart, B.D. Sykes, The 13C chemical-shift index: a simple method for the identification of protein secondary structure using 13C chemical-shift data, J. Biomol. NMR 4 (1994) 171–180.
[19] K. Wuthrich, NMR of Proteins and Nucleic Acids, John Wiley & Sons, New York, 1986.
[20] N.H. Anderson, J.W. Neidigh, S.M. Harris, G.M. Lee, Z. Liu, H. Tong, Extracting information from the temperature gradients of polypeptide HN chemical shifts. 1. The importance of conformational averaging, J. Am. Chem. Soc. 119 (1997) 8547–8561.
[21] N.J. Baxter, M.P. Williamson, Temperature dependence of 1H chemical shifts in proteins, J. Biomol. NMR 9 (1997) 359–369.
[22] F. Cordier, S. Grzesiek, Temperature-dependence of protein hydrogen bond properties as studied by high-resolution NMR, J. Mol. Biol. 317 (2002) 739–752.
[23] M.E. Daley, S.P. Graether, B.D. Sykes, Hydrogen bonding on the ice-binding face of a beta-helical antifreeze protein indicated by amide proton NMR chemical shifts, Biochemistry 43 (2004) 13012–13017.
[24] H.J. Dyson, M. Rance, R.A. Houghten, R.A. Lerner, P.E. Wright, Folding of immunogenic peptide fragments of proteins in water solution. I. Sequence requirements for the formation of a reverse turn, J. Mol. Biol. 201 (1988) 161–200.
[25] M. Ohnishi, D.W. Urry, Temperature dependence of amide proton chemical shifts: the secondary structures of gramicidin S and valinomycin, Biochem. Biophys. Res. Commun. 36 (1969) 194–202.
[26] G. Wagner, A. Pardi, K. Wuthrich, Hydrogen bond length and ^{1}H NMR chemical shifts in proteins. J. Am. Chem. Soc. 105 (1983) 5948–5949.
[27] T. Cierpicki, J. Otlewski, Amide proton temperature coefficients as hydrogen bond indicators in proteins, J. Biomol. NMR 21 (2001) 249–261.
[28] R.F. Tilton Jr., J.C. Dewan, G.A. Petsko, Effects of temperature on protein structure and dynamics: X-ray crystallographic studies of the protein ribonuclease-A at nine different temperatures from 98 to 320 K, Biochemistry 31 (1992) 2469–2481.
[29] T. Cierpicki, I. Zhukov, R.A. Byrd, J. Otlewski, Hydrogen bonds in human ubiquitin reflected in temperature coefficients of amide protons, J. Magn. Reson. 157 (2002) 178–180.
[30] M.P. Williamson, Many residues in cytochrome c populate alternative states under equilibrium conditions, Proteins 53 (2003) 731–739.

[31] N. Hirokawa, Y. Noda, Y. Okada, Kinesin and dynein superfamily proteins in organelle transport and cell division, Curr. Opin. Cell Biol. 10 (1998) 60–73.
[32] E.L. Holzbaur, R.B. Vallee, DYNEINS: molecular structure and cellular function, Annu. Rev. Cell Biol. 10 (1994) 339–372.
[33] S. Karki, E.L. Holzbaur, Cytoplasmic dynein and dynactin in cell division and intracellular transport, Curr. Opin. Cell Biol. 11 (1999) 45–53.
[34] S.M. King, The dynein microtubule motor, Biochim. Biophys. Acta 1496 (2000) 60–75.
[35] M.P. Koonce, M. Samso, Of rings and levers: the dynein motor comes of age, Trends Cell Biol. 14 (2004) 612–619.
[36] R.B. Vallee, M.P. Sheetz, Targeting of motor proteins, Science 271 (1996) 1539–1544.
[37] K.K. Pfister, Dynein cargo gets its groove back, Structure 13 (2005) 172–173 (Camb.).
[38] S.M. King, E. Barbarese, J.F. Dillman III, S.E. Benashski, K.T. Do, R.S. Patel-King, K.K. Pfister, Cytoplasmic dynein contains a family of differentially expressed light chains, Biochemistry 37 (1998) 15033–15041.
[39] T. Dick, K. Ray, H.K. Salz, W. Chia, Cytoplasmic dynein (ddlc1) mutations cause morphogenetic defects and apoptotic cell death in *Drosophila melanogaster*, Mol. Cell. Biol. 16 (1996) 1966–1977.
[40] K.F. Hoffmann, M. Strand, Molecular identification of a *Schistosoma mansoni* tegumental protein with similarity to cytoplasmic dynein light chains, J. Biol. Chem. 271 (1996) 26117–26123.
[41] S.M. King, R.S. Patel-King, The $M(r)=8000$ and 11,000 outer arm dynein light chains from *Chlamydomonas* flagella have cytoplasmic homologues, J. Biol. Chem. 270 (1995) 11445–11452.
[42] P.M. Mohan, M. Barve, A. Chatterjee, R.V. Hosur, pH driven conformational dynamics and dimer-to-monomer transition in DLC8, Protein Sci. 15 (2006) 335–342.
[43] W. Wang, K.W. Lo, H.M. Kan, J.S. Fan, M. Zhang, Structure of the monomeric 8-kDa dynein light chain and mechanism of the domain-swapped dimer assembly, J. Biol. Chem. 278 (2003) 41491–41499.
[44] J. Liang, S.R. Jaffrey, W. Guo, S.H. Snyder, J. Clardy, Structure of the PIN/LC8 dimer with a bound peptide, Nat. Struct. Biol. 6 (1999) 735–740.
[45] M. Makokha, Y.J. Huang, G. Montelione, A.S. Edison, E. Barbar, The solution structure of the pH-induced monomer of dynein light-chain LC8 from *Drosophila*, Protein Sci. 13 (2004) 727–734.
[46] H.S. Atreya, K.V. Chary, Selective 'unlabeling' of amino acids in fractionally 13C labeled proteins: an approach for stereospecific NMR assignments of CH3 groups in Val and Leu residues, J. Biomol. NMR 19 (2001) 267–272.
[47] P. Permi, Coherence transfer in proteins, Prog. Nucl. Magn. Reson. Spectrosc. 44 (2004) 97–137.
[48] V. Tugarinov, P.M. Hwang, L.E. Kay, Nuclear magnetic resonance spectroscopy of high-molecular-weight proteins, Annu. Rev. Biochem. 73 (2004) 107–146.
[49] F.A. Mulder, A. Mittermaier, B. Hon, F.W. Dahlquist, L.E. Kay, Studying excited states of proteins by NMR spectroscopy, Nat. Struct. Biol. 8 (2001) 932–935.
[50] A.E. Ferentz, G. Wagner, NMR spectroscopy: a multifaceted approach to macromolecular structure, Q. Rev. Biophys. 33 (2000) 29–65.
[51] S.C. Panchal, N.S. Bhavesh, R.V. Hosur, Improved 3D triple resonance experiments, HNN and HN(C)N, for HN and 15N sequential correlations in (13C, 15N) labeled proteins: application to unfolded proteins, J. Biomol. NMR 20 (2001) 135–147.
[52] P.M. Krishna Mohan, Unfolding energetics and conformational stability of DLC8 monomer, Biochimie 89 (2007) 1409–1415.
[53] N.J. Baxter, L.L. Hosszu, J.P. Waltho, M.P. Williamson, Characterisation of low free-energy excited states of folded proteins, J. Mol. Biol. 284 (1998) 1625–1639.
[54] K. Akasaka, Probing conformational fluctuation of proteins by pressure perturbation, Chem. Rev. 106 (2006) 1814–1835.
[55] A. Nyarko, L. Cochrun, S. Norwood, N. Pursifull, A. Voth, E. Barbar, Ionization of His 55 at the dimer interface of dynein light-chain LC8 is coupled to dimer dissociation, Biochemistry 44 (2005) 14248–14255.
[56] P.M. Krishna Mohan, R.V. Hosur, NMR insights into dynamics regulated target binding of DLC8 dimer, Biochem. Biophys. Res. Commun. 355 (2007) 950–955.
[57] J. Fan, Q. Zhang, H. Tochio, M. Li, M. Zhang, Structural basis of diverse sequence-dependent target recognition by the 8 kDa dynein light chain, J. Mol. Biol. 306 (2001) 97–108.
[58] J.J. Spitzer, B. Poolman, Electrochemical structure of the crowded cytoplasm, Trends Biochem. Sci. 30 (2005) 536–541.
[59] A.K. Stewart, C.A. Boyd, R.D. Vaughan-Jones, A novel role for carbonic anhydrase: cytoplasmic pH gradient dissipation in mouse small intestinal enterocytes, J. Physiol. 516 (Pt 1) (1999) 209–217.
[60] P. Swietach, C.H. Leem, K.W. Spitzer, R.D. Vaughan-Jones, Experimental generation and computational modeling of intracellular pH gradients in cardiac myocytes, Biophys. J. 88 (2005) 3018–3037.
[61] R.D. Vaughan-Jones, B.E. Peercy, J.P. Keener, K.W. Spitzer, Intrinsic H(+) ion mobility in the rabbit ventricular myocyte, J. Physiol. 541 (2002) 139–158.
[62] D. Willoughby, C.J. Schwiening, Electrically evoked dendritic pH transients in rat cerebellar Purkinje cells, J. Physiol. 544 (2002) 487–499.
[63] A. Chatterjee, P.M. Krishna Mohan, A. Prabhu, A. Ghosh-Roy, R.V. Hosur, Equilibrium unfolding of DLC8 monomer by urea and guanidine hydrochloride: Distinctive global and residue level features, Biochimie 89 (2007) 117–134.